Magnetic Resonance in Medicine 66:135–143 (2011)

Head Motion Detection Using FID Navigators

Tobias Kober,[1,2,3]* José P. Marques,[1,2] Rolf Gruetter,[1,2,4] and Gunnar Krueger[3]

This work explores a concept for motion detection in brain MR examinations using high channel-count RF coil arrays. It applies ultrashort (<100 μsec) free induction decay signals, making use of the knowledge that motion induces variations in these signals when compared to a reference free induction decay signal. As a proof-of-concept, the method was implemented in a standard structural MRI sequence. The stability of the free induction decay-signal was verified in phantom experiments. Human experiments demonstrated that the observed variations in the navigator data provide a sensitive measure for detection of relevant and common subject motion patterns. The proposed methodology provides a means to monitor subject motion throughout a MRI scan while causing little or no impact on the sequence timing and image contrast. It could hence complement available motion detection and correction methods, thus further reducing motion sensitivity in MR applications. Magn Reson Med 66:135–143, 2011. © 2011 Wiley-Liss, Inc.

Key words: MRI; motion detection; FID navigators; head imaging; multicoil arrays

During the previous three decades, magnetic resonance imaging (MRI) has evolved into one of the most important medical imaging techniques. Compared to other imaging methods used for clinical diagnosis, MRI benefits especially from its excellent soft-tissue contrast. MRI protocols, however, require long acquisition times, implicating strong motion sensitivity. This is even more critical when examining less cooperative, elderly or impaired patients with reduced tolerance for long acquisitions. Resulting motion artefacts lead to a degradation of image quality, often rendering them useless for diagnosis. Recently, various methodologies have been proposed to overcome motion sensitivity and to correct motion in MR brain scans.

In rapid single-shot acquisitions, prospective motion correction schemes have been implemented (1,2). They make use of the fact that the whole acquisition volume can be scanned within seconds. Subsequently, acquired volumes are coregistered in quasi real-time and can be used to feed back motion parameters to the MR system for prospective adaptation of the gradient coordinate system (2). Other approaches use external optical devices to track patient motion (3,4); this information can then also be used prospectively in quasi real-time. Furthermore, alternative data acquisition strategies, which are less prone to motion artefacts (mostly due to oversampling of the *k*-space centre) such as projection reconstruction (5), spiral imaging (6), or PROPELLER (7), have been applied to cope with subject motion.

An attractive, but typically more time-consuming approach to address motion in MRI is the use of navigator data. Navigators have been used to detect and correct for motion in a number of MR applications ranging from structural to cardiac imaging. They have been continuously developed since their introduction by Ehman and Felmlee in 1989 (8), namely orbital (2D) and spherical (3D) navigators (9–13) as well as spiral-based ones (14). Recently, navigators have been extended to measure effects like motion-induced shim changes [e.g. Refs. 15,16]. Some applications were also shown for spectroscopic acquisitions (17).

All these methods have in common that the additional information comes along with increased scan times and that they are, in some cases, limited in the achievable quality and resolution or imply perturbations of the steady state magnetization due to additional excitation RF-pulses. In particular, the additional RF-pulse renders navigator echoes often inappropriate for fast imaging techniques like FLASH (18) or RARE (19).

In contrast, free induction decay (FID) navigators, which monitor the k-space centre without any spatial encoding, have minimal or no impact at all on the imaging procedure and hence the scan time. Originally developed to correct B_0 drifts and fluctuations in fMRI caused by respiratory movements and system instabilities (20,21), a recent approach uses them to gain up to second order shim information (22). Brau and Brittain introduced the concept of motion monitoring using the DC component of the FID signal and used it for prospectively gated abdominal acquisitions (23).

Extending previous reports on DC- and FID-navigators, this work investigates the potential to monitor head motion using ultrashort (<100 μsec) FID navigators from multiple coil elements. In a first application, results from a real-time rescanning framework implemented in an anatomical imaging sequence are shown.

MATERIALS AND METHODS

Theory

During the past decade, multichannel coil arrays became widely used in clinical MR examinations. Here, a commercial 32-channel head coil array based on a design as proposed recently (24) is used. Such a coil design is

[1]Laboratory for Functional and Metabolic Imaging, Ecole Polytechnique Fédérale de Lausanne, Switzerland.

[2]Department of Radiology, University of Lausanne, Lausanne, Switzerland.

[3]Siemens Schweiz AG, Healthcare Sector IM&WS S, Renens, Switzerland.

[4]Department of Radiology, University of Geneva, Geneva, Switzerland.

Grant sponsors: Centre d'Imagerie BioMédicale (CIBM) of the University of Lausanne (UNIL), the Swiss Federal Institute of Technology Lausanne (EPFL), the University of Geneva (UniGe), the Centre Hospitalier Universitaire Vaudois (CHUV), the Hôpitaux Universitaires de Genève (HUG), and the Leenaards and the Jeantet Foundations.

*Correspondence to: Tobias Kober, M.S., Ecole Polytechnique Fédérale de Lausanne, LIFMET-CIBM, Station 6, 1015 Lausanne, Switzerland. E-mail: tobias.kober@epfl.ch

Received 8 June 2010; accepted 9 December 2010.

DOI 10.1002/mrm.22797

Published online 17 February 2011 in Wiley Online Library (wileyonlinelibrary.com).

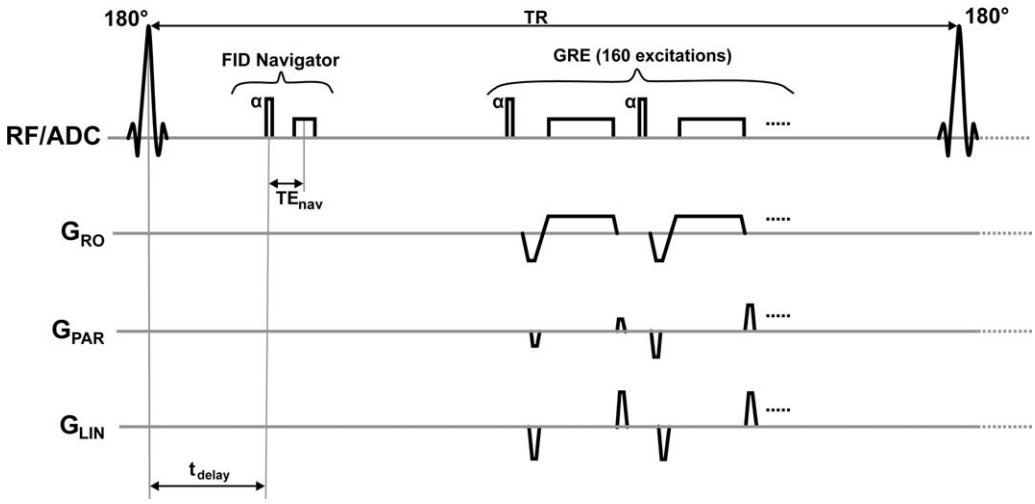

FIG. 1. Diagram of the modified MP-RAGE sequence. One FID navigator excitation is added $t_{delay} = 50$ msec after the inversion pulse. The flip angle $\alpha = 9^\circ$ is the same as the one of the imaging scans, navigator echo time TE_{nav} is 1 msec. No gradients are applied in the navigator module, yielding whole-volume FID data.

ideal for the approach under investigation as it comprehensively covers the subject's head.

An interesting aspect of multichannel coil arrays, which is exploited in this work, is the dependency of the received MR signal strength and phase on the object's distance from an individual coil element. Considering only a single coil element, it is evident that changes in object position, i.e. head motion away or towards the coil, may result in changes of the received MR signal. Similarly, phase changes in the MR signal may also encode motion information, as motion often changes the B_0 field pattern due to the changed position of the susceptibility gradients in the skull as well as to the inherent phase coil sensitivity. For the single-coil-element case, the relationship between distance and signal strength can be calculated by means of the electromagnetic laws. In a realistic in vivo experiment, however, various interferences (loading, head geometry, coil coupling and others) render an analytical approach unfeasible. Hence, our method is heuristically derived from experimental data.

To detect motion, this technique uses short samples of a FID—herein referred to as FID navigators—from all coil elements to detect motion. The FID navigators are acquired at each TR during the measurement without application of any spatial gradient encoding.

MR Equipment and Test Setup

All experiments were performed on a clinical 3T scanner (Magnetom Trio a Tim System, Siemens Healthcare, Erlangen, Germany) equipped with a product 32-channel receive head coil array.

A product 3D MP-RAGE sequence was modified to include an FID navigator block 50 msec after the inversion pulse (cf. Fig. 1). It comprised a dedicated nonselective excitation pulse followed by an ADC readout in the absence of gradients. The same (nonselective) rect-pulse (flip angle $\alpha = 9^\circ$) was applied in the FLASH imaging block. The FID navigator sampled 40 points in 83 μsec (240 Hz/pixel) at an echo time of $TE_{nav} = 1$ msec. To remove effects due to electronic adjustments of the analogue-digital-converter (ADC), only the last 30 sample points were averaged, yielding one complex value per coil element and time point.

The parameters of the modified MP-RAGE sequence used for both phantom and human experiments were as follows: TR = 2200 msec, TI = 900 msec, $TE_{GRE} = 2.8$ msec, echo-spacing 6.6 msec, bandwidth 240 Hz/pixel, 240 × 256 × 160 matrix with isotropic voxel size of 1 mm and nonselective inversion and excitation pulses [adapted from ADNI protocol (25)]. The resulting acquisition time was 9:14 min.

As the navigator was placed in the delay time between the inversion pulse and the beginning of the FLASH imaging readout block, the repetition time TR and the overall protocol duration remained unaffected by the FID navigator module.

Bloch simulations were performed and showed only negligible effects on the entire magnetization arising from the introduced FID RF-pulse with <0.2% at the inversion time TI = 900 msec as in the applied protocol.

Phantom Experiments

Subject motion may induce changes in the FID signal amplitude and phase. Beyond that, navigator signal stability can also be affected by physiological processes from respiration and cardiac cycles as well as by system fluctuations arising from hardware instabilities. Hardware and thermal effects may cause B_0 drifts and changes in RF-pulse amplitude, loading etc. Those fluctuations (apart from possible physiological respiratory effects) were evaluated in phantom experiments to quantify the obtainable stability of the navigator signal. All phantom experiments were conducted using the modified MP-RAGE sequence and a 7.3-L cylindrical water phantom (1.25 g $NiSO_4 \times 6\ H_2O$/2.62 g NaCl per 1000 g H_2O), which provides a coil loading comparable to that

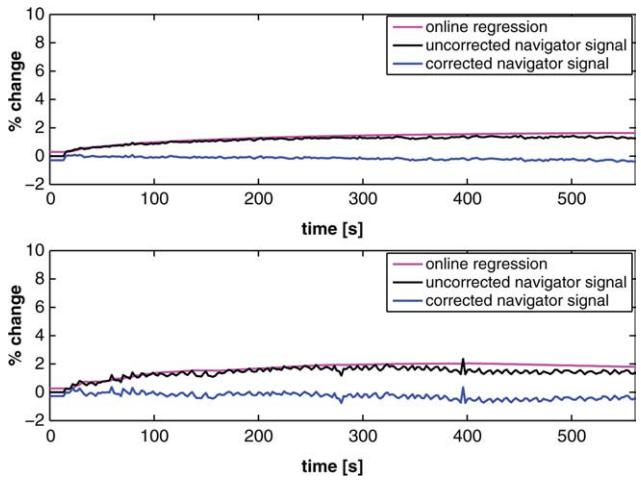

FIG. 2. Navigator signals of an exemplary phantom (top) and human rest (bottom) experiment: uncorrected signal (black), the online regression points (magenta/light grey), and the resulting corrected navigator (blue/dark grey). Note that the slope is higher at the beginning, supposedly caused by thermal effects. [Color figure can be viewed in the online issue, which is available at wileyonlinelibrary.com.]

of a human head. Standard deviations and peak-to-peak amplitude as well as linear slopes of the navigator time series were determined (cf. Fig. 2).

Motion Detection Algorithm

An algorithm for detection of head motion based on navigator signals was developed and implemented in the scanner reconstruction pipeline as a real-time feedback routine.

With each TR, the 30 complex FID points are averaged to obtain one complex FID data point for each coil element. In the current implementation, navigator signals are acquired once per TR = 2200 msec (in case of MP-RAGE defined as the time interval between two inversion pulses, see Fig. 1). Because the longitudinal magnetization reaches its steady state only after a few TRs, FID data from the first three TRs are discarded. The navigator signals of the following five repetitions are used to accumulate (complex) reference data ref_i for each coil element i. Hence, the initial <18 sec of the scan are used for self-adjustment of the motion detection.

For determination of a global motion parameter indicating subject motion, the navigator signals of the different coil elements are combined, and subsequently, a mean percentage change $\Delta(n)$ to the reference points is calculated as follows:

$$\Delta(n) = \frac{1}{N}\sum_{i=1}^{N}\frac{|\mathrm{nav}_i(n) - \mathrm{ref}_i|}{|\mathrm{ref}_i|}$$

where n is the repetition number, N the number of coil elements, and $\mathrm{nav}_i(n)$ is the complex navigator data of coil element i in repetition number n. Note that such data combination results in a single motion sensitivity parameter Δ per repetition; it is interpreted as a mean per cent change to the reference points from the beginning of the scan. Consequently, a simple threshold criterion can be applied to Δ, facilitating real-time execution of the motion-detection algorithm.

To account for system-induced instabilities (e.g., slow drifts) and to improve robustness of the detection algorithm throughout the experiment, the motion threshold criterion is updated in an adaptive manner. Figure 3 depicts the procedure: each incoming data navigator point $\Delta(n)$ is compared to a point linearly extrapolated from all preceding points, which are included in the regression time-course at that point in time. If the incoming navigator point $\Delta(n)$ exceeds three times the standard deviation of all points in the regression time course (i.e., it is outside a 99.7% confidence interval for a normal distribution), the corresponding repetition (and thus k-space line) is considered as significantly affected by motion and labelled "motion-corrupted." The corresponding navigator information of those scans is subsequently excluded from the regression time course. This assures that motion-corrupted navigator signals do not affect the further linear extrapolation as well as the dynamic threshold calculation in successive repetitions.

In the phantom experiments (using the same protocol parameters as applied in the human experiments), a maximal system-induced drift of 0.9%/min was observed. Accordingly, this value is configured as a maximal slope in the linear regression, i.e., a low frequency evolution up to 0.9%/min is not interpreted as subject motion in the in vivo scans. The difference between the navigator time course $\Delta(n)$ and the online regression curve will be referred to as the "corrected navigator signal" throughout this work; it represents the navigator signal after correction of system-induced drifts and will, therefore, be used for further quantification of the signal stability.

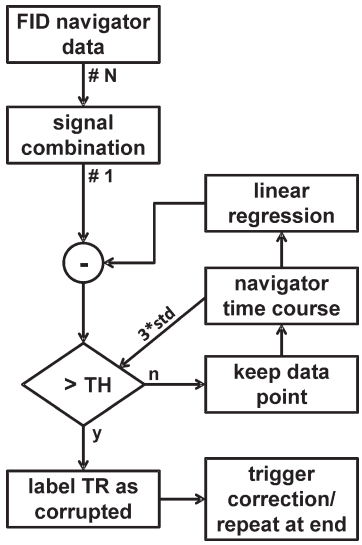

FIG. 3. Motion detection algorithm: incoming navigator data are combined and then tested against a data point linearly extrapolated from previous navigator time course. The latter also defines the adaptive threshold. Only if a navigator point is below this threshold, it is kept in the time course for calculation of the subsequent regression and threshold. Otherwise, the repetition is labelled as motion-corrupted while discarding the navigator data of this repetition.

In the current proof-of-concept setup, all repetitions labelled "motion-corrupted" were automatically repeated at the end of the scan until all *k*-space lines were labelled "motion-free." This condition may not be fulfilled in a real human experiment. However, it is a very difficult task to accurately quantify subject motion in MR experiments and the chosen procedure with voluntary, trained back-and-forth motion patterns allowed investigating the capability of the method in a more controlled fashion.

In Vivo Experiments

In total, five healthy subjects (25 ± 5 years) were scanned in accordance with the local ethic protocol. All subjects provided written informed consent.

After positioning in the 32-channel head coil, subjects were instructed to perform and train a movement between two different head positions R ("rest") and M ("moved"), which they could reliably repeat. For good reproducibility of the motion performed, subjects underwent a motion training phase during which they were asked to move repeatedly from position R to position M and vice versa, while an EPI acquisition with online rigid-body registration was performed (3:26 min, 32 slices, 64 × 64 matrix, TR 2.2 sec). The online calculation of motion parameters and motion monitoring using the vendor's volume-registration based motion-detection software (2) allowed for controlling the extent of the motion and the precision of repositioning. If the precision or the extent of motion was not satisfactory, the motion learning phase was repeated after giving verbal feedback to the Subject. Using this procedure, all subjects trained a motion paradigm with a maximum of 5 mm translation and 7° rotation on any of the axes and managed to reach reproducibility within 1 mm and 1°.

Before the start of the 9-min structural scan with the modified MP-RAGE sequence, subjects were asked to move their head to position R. During scanning, subjects were verbally instructed after 4 min (close to k-space centre) to move their head to position M and, 1 min later, to move it back to position R. A second MP-RAGE scan was subsequently acquired without voluntary motion. Directly before and after both MP-RAGE scans, short EPI acquisitions were performed (five volumes, same EPI parameters as above) to further evaluate the head repositioning via volume coregistration of the EPI volumes. Note that in both motion-corrupted and rest MP-RAGE scans, the online FID motion detection algorithm was activated.

Furthermore, different head movements were tested on one subject to ensure that common motion patterns are equally detected by the presented method. The following head movements were chosen: (a) rotation about *x*-axis (nod movement), (*b*) rotation about *z*-axis (head-shaking movement), and (c) translation in *z*-direction (inferior-superior, a component of neck muscle relaxation after positioning). For all the three motion patterns, a motion training phase as described above was performed. For (a) and (c), a shorter MP-RAGE protocol was used (256 × 256 × 64 matrix, thus only 64 repetitions, TR = 2.2 sec, resulting TA = 2:24 min); here, only the extent of the navigator signal change with respect to the performed motion was investigated. Movement (b) was performed during the motion MP-RAGE scan of the standard measurement protocol.

RESULTS

Navigator Signal Stability

Phantom experiments occasionally revealed measurable drifts in the FID navigator signals $\Delta(n)$, which were attributed to system-induced fluctuations and largely of linear character (see a typical time course in Fig. 2). In some experiments, however, the slope of the navigator signal time course was increased at the beginning of the measurement and dwindled to a constant slope after 20–30 sec, suggesting thermal effects as a likely cause. Both drift behaviors were compensated by the online regression algorithm, yielding corrected time courses.

In phantom scans, the mean drift slope over 9:14 min of all experiments was 0.13%/min (ranging from 0.002 to 0.27%/min intraexperiment means), with a maximal slope during a 1 min window of 0.9%/min. The maximum slope was observed in early scan phases where thermal effects seem to be relevant (see Fig. 2, time = 0–100 sec) and introduced as the maximal allowed system-induced low frequency slope in the motion detection algorithm (see Methods section).

In vivo navigator MP-RAGE experiments without motion confirmed the observation from the phantom experiments that the navigator signal may be subject to slight system-induced drift; its slopes here were on average 0.06%/min (ranging from 0.006 to 0.18%/min intraexperiment means).

The corrected (i.e., free of systematic drifts) time courses of the phantom experiments showed excellent stability with a maximum sd = 0.25% and a mean peak-to-peak amplitude of 0.80%. The analysis of the performed human experiments without motion confirmed the results reported above. As it can be seen in the time course in Fig. 2, bottom system drifts could be well compensated in in vivo experiments. The mean standard deviation of the corrected navigator signals for all human rest experiments was sd = 0.30% (uncorrected: 0.38%), their mean peak-to-peak amplitude 1.62%. The higher values in in vivo experiments are expected as they also reflect higher noise levels when using a biological loading, but also physiological processes (e.g. breathing and cardiac cycles) and residual motion which might have appeared unintentionally. To account for possible system-induced temporal signal variations, the algorithm allowed a maximum signal drift of 0.9%/min; exceeding signal changes were attributed to subject motion.

Minimal Duration of Navigator

To investigate the time limits of the FID navigators, the acquired data was reconstructed using only a subset of the 40 sampled points. Thereby, the first point was always omitted because it was found to be partially corrupted by noise. Good results could still be achieved, however, using only the second and the third point sampled (the root mean squared difference compared to using all points amounts to 0.04%). Assuming the same

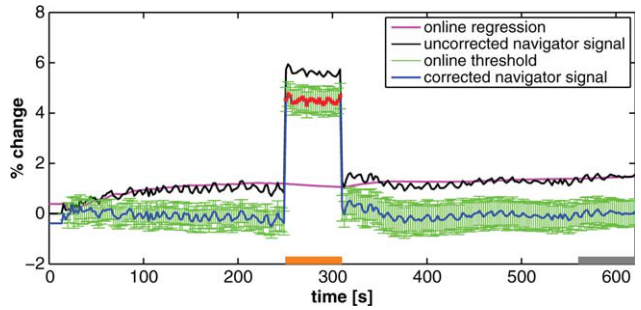

FIG. 4. Navigator time course of in vivo experiment with motion, which was performed during the period marked with the orange bar. *K*-space lines considered "motion-corrupted" by the online algorithm are marked in red. The according *k*-space lines were automatically repeated at the end of the scan (grey bar).

bandwidth which was used in the MP-RAGE sequence, this result suggests that FID navigators as short as 6 μsec provide sufficient information to be used with the present technique, even with a low flip-angle excitation like the one applied here (9°).

In Vivo Experiments with motion

In all experiments, head movements were reliably detected with the implemented algorithm. The performed movements resulted in FID navigator signal changes between 2 and 9 percentage points in the human experiments. An exemplary navigator time course can be seen in Fig. 4 (underlying motion trans = 2 mm and rot = 5°). The other acquisitions showed similar time courses. Confirming that subjects were able to perform the movement and return to position R, the labelling of the motion-corrupted *k*-space lines and reacquisition at the end worked in all subject scans. Hence, in all cases MP-RAGE images could be reconstructed both with motion-corrupted and with uncorrupted *k*-space lines. Figure 5 displays sagittal MP-RAGE images from all subjects: the first column and the cut-out in the second column show reconstructions using

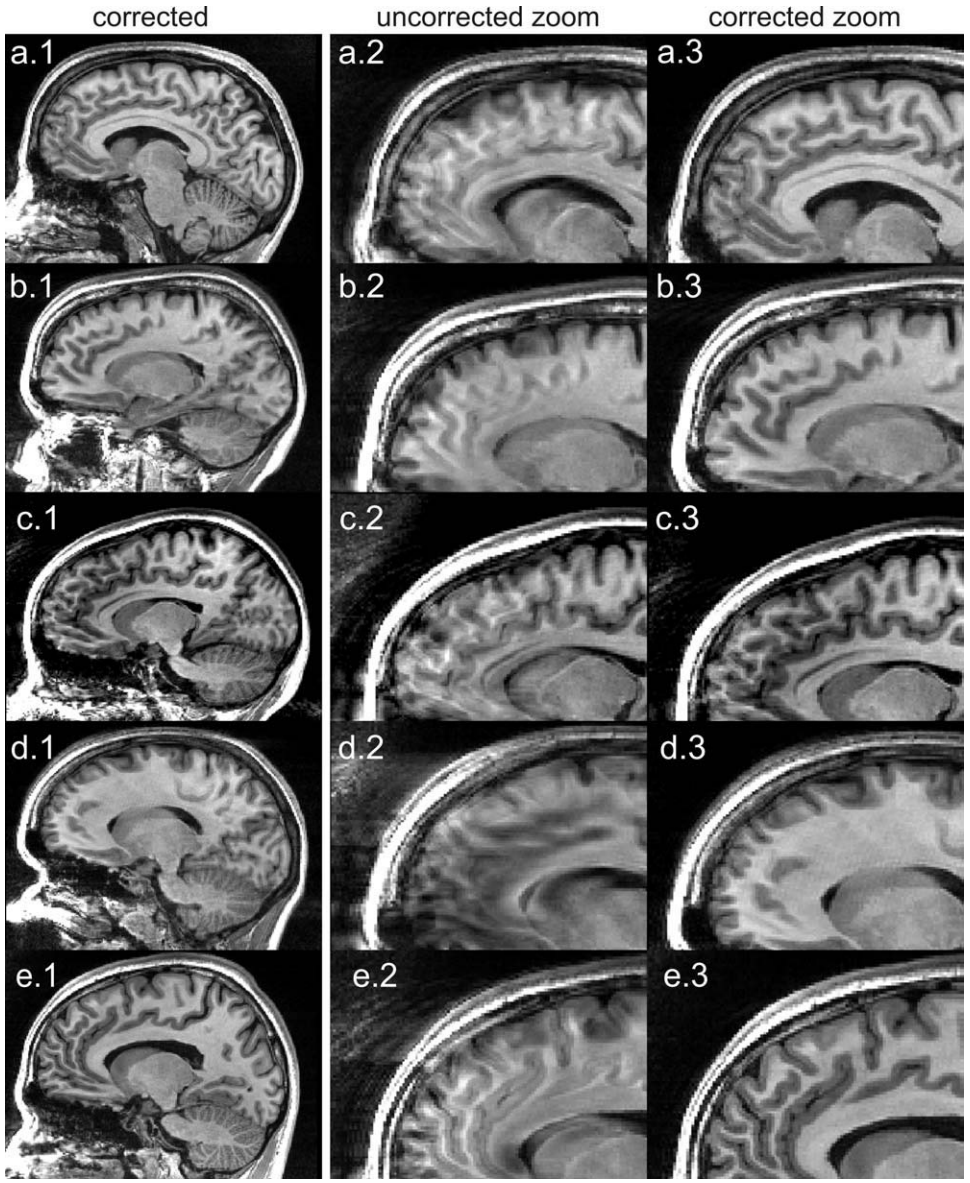

FIG. 5. First column: whole-head sagittal MP-RAGE images from all five subjects (**a**–**e**) using the repeated *k*-space data. Second and third column: cut-outs of the same slice reconstructed using the *k*-space data marked as motion corrupted during the scan (second column) and, for comparison, the same cut-out of the images using the repeated *k*-space data (third column). Images e.1–3 depict the data corresponding to the navigator course shown in Figure 4. Windowing is kept constant within subjects.

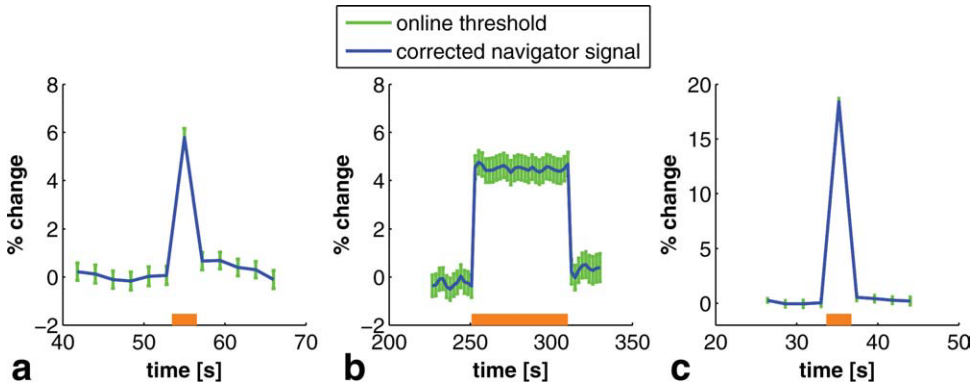

FIG. 6. Navigator time courses (blue) for three different motion patterns (vertical bars show online threshold). The performed movements were "nodding" (rotation about *x*-axis, **a**), "head-shaking" (rotation about *z*-axis, **b**) and z-translation (**c**). The horizontal bars at the bottom show the period during which the movement was performed (forth and back). [Color figure can be viewed in the online issue, which is available at wileyonlinelibrary.com.]

the repeated (i.e., uncorrupted) lines from the end of the scan, whereas the images in the third column were reconstructed using the corrupted *k*-space lines.

The different motion patterns tested on one subject confirmed that the motion detection worked for all common head movements. As stated above, the following motion patterns were tested: (a) rotation about *x*-axis (nod movement), (b) rotation about *z*-axis (head-shaking movement), and (c) translation in *z*-direction (inferior-superior). Figure 6 shows the navigator signal changes from the three motion patterns. All different motion patterns caused a significant change of the navigator signal, which was reliably detected by the algorithm. Although for these patterns only partial *k*-space data were acquired, the results indicate that the proposed motion detection works also for other movements.

Table 1 shows the movements performed by the subjects and its impact on the navigator signal. From the threshold used, we can conclude that the current motion detection scheme would probably be able to detect much smaller movements. If a linear relationship between navigator amplitude change and motion is assumed for each subject, then a fraction in the order of $\tau/\Delta_{\text{navigator}}$ of the performed movement could have been detected.

Image Quality Assessment

To compare the corrected and uncorrected images quantitatively, an automated quality assessment method developed by Mortamet et al. (26) was used. The generated quality indices confirmed the visible improvement in the corrected images: in all cases the algorithm rated images reconstructed with the corrupted *k*-space lines with lower image quality than the ones reconstructed with the corrected *k*-space lines (the quality index improved between 13 and 47%, mean improvement: 22%).

DISCUSSION

The presented results prove the feasibility of the proposed method to detect motion. As demonstrated with a MP-RAGE approach, the method allows motion detection with little or no time-penalty. Note that this application was chosen to show the entire implementation of a real-time FID navigator feedback loop, while keeping the mechanism itself and the sequence design as clear and simple as possible. The technique is yet considered to be compatible with a variety of other sequences. As stated above, it does not require an extra navigator excitation but can rather be inserted after the existing excitation pulse of the host sequence, yielding minimal time penalty. A navigator being as short as 6 μsec can contain enough information to detect occurred head motion. The method is furthermore considered to have particular potential for MR schemes where normal motion correction schemes are difficult to apply, such as diffusion imaging, contrast-enhanced perfusion or spectroscopy. In the following, we will discuss its limitations, possible improvements, and future applications.

Minimal FID Navigator Duration

In the presented application, the FID navigators used a separate excitation pulse and were sampled for 83 μsec. This approach was chosen because of the inherent idle time between the inversion pulse and the FLASH readout in MP-RAGE sequences, i.e., time was not a critical issue in this sequence scheme. Furthermore, the separate excitation pulse used had only a negligible effect on the

Table 1
Motion Impact on Navigator Signal for the Five Subjects Scanned

Subject no.	rot [°]	trans [mm]	$\Delta_{\text{navigator}}$ [p. p.]	τ [p. p.]
#1	2.8	1.5	4.6	0.60
#2	3.8	1.8	1.4	0.41
#3	7.1	3.2	4.2	0.50
#4	5.8	5.4	6.9	0.41
#5	4.9	2.1	4.7	0.48

The movement parameters shown are assumed to be the same as those during the training period and were calculated from the corresponding EPI scans using rigid body coregistration (only the total translation, "trans," and the primarily contributing rotation component, "rot," are shown). $\Delta_{\text{navigator}}$ (Column 4) represents the change in the corrected navigator seen immediately before and after the movement occurred. The values of the threshold, τ, correspond to three times the standard deviation of the corrected navigator at the time motion was performed.

imaging signal. If the navigator would be used in a different sequence, however, timing might become more crucial. In imaging schemes without magnetization preparation (e.g., FLASH sequences), the excitation pulse of the host sequence could directly be used to sample the FID information with minimal effects on the overall sequence timing. The FID navigator ADC had to be simply "squeezed" in the sequence scheme accordingly. For a 3D structural brain FLASH scan, for instance, the TE would be prolonged by <0.5 msec. In such cases, the sampling of the FID should obviously be as short as possible

The presented results showed a root mean squared difference of only 0.04% between the navigator time course obtained by averaging over all sampled points and the one averaged over the second and third point (resulting in 6 μsec sampling duration). This suggests that FID navigators as short as 10 μsec can provide robust information of patient motion while (i) having negligible impact on the steady-state magnetization, (ii) being contrast-independent, and (iii) if applied in a deliberated manner, are providing a very time-efficient implementation with no or only little time-penalties. In the current concept, combined signals from a 32-channel coil were used; though intuitively a higher number of coil elements might provide a higher sensitivity to detect motion, future work should also investigate in more detail the optimal number of coil elements and their spatial distribution to be used for such an approach.

Respiration-Induced Signal Changes

As shown in van de Moortele et al. (27), respiration induces B_0 shifts even at the level of the brain. As reported there, the resulting phase shifts in the FID navigator range between 7 Hz at the brain stem to 1 Hz at the top of the brain at 7 T. Scaling this effect down to 3 T and considering the average effect over the whole brain (assuming a cubic decay), the phase shift would be of the order of <1 Hz. Such a peak-to-peak frequency variation would imply a phase variation on our navigator acquired at an echo time of 1 msec of 0.3° while keeping its magnitude unchanged. The maximum $\Delta(n)$ attributable to respiration would be 0.6%, suggesting that the navigator peak-to-peak amplitude should decrease if $\Delta(n)$ was calculated using only magnitude signals. And indeed, the peak-to-peak amplitude averaged over all human rest scans drops from 1.6 to 0.9% when excluding the phase information (the latter being close to the 0.8% obtained in phantom scans with the phase-sensitive algorithm). This decreased noise level results, however, also in a decreased sensitivity to motion (as we observed if the human scans with motion were processed with the phase-insensitive algorithm).

In conclusion, it is very likely that the additional noise in the navigator signal is partly due to respiration-induced B_0 shifts. The adaptive threshold, however, ensures that these shifts are not falsely detected as motion.

Slice-Selective Excitations

In the presented implementation, the navigator monitors a nonselectively excited FID. Consequently, the navigator signals acquired each TR are comparable among themselves. If the navigator is incorporated in a 2D sequence, however, the FID signals would contain information from the selected slice and exhibit sensitivity according to the different excited spatial locations. The decreased signal strengths OF some of the FID navigators might, however, be counterbalanced by a higher sensitivity due to a much more localized excitation volume compared with the whole-volume-excitation case. This might yield an even higher change in the navigator signal. Nevertheless, further investigations are necessary to examine the effects of a 2D implementation.

Experimental Setup

The primary goal of the presented setup was to show the feasibility of the method to detect motion within a straightforward and simple framework in an application where a clinical need exists. Although the current experimental setup does not meet the requirements of a realistic clinical scenario, the motivation of this article was to develop and to explore the potential of the approach for motion detection. A key finding is that the navigator signal changes were found to reveal motion with a sensitivity that—if corrected—would significantly improve image quality. The reliable detection of motion is thereby seen as a first step to improve quality of clinical scans (note that occurred motion was detected in all cases). In its most simple use, the information of detected motion could be used to initiate an immediate quality rating of the scan by a technician or to calculate a quality index (26), which could subsequently result in a rescan.

In a more realistic setting, a motion correction procedure would be initiated after motion detection. For example, the acquisition of an EPI volume could be initiated after detection of significant motion within one TR of a structural scan, similar to a recently proposed approach (28). The EPI volume could be registered to a volume acquired at the beginning of the scan, providing the motion parameters to adapt the imaging gradient system accordingly. With necessary pulses to attain steady-state magnetization once more, this correction could be accomplished in a few seconds. The MP-RAGE scan could then be continued by rescanning the last repetition.

Recently, it has been shown that inaccuracy and noise in quantification of motion parameters may result in image artefacts if used for correction (29). For clinical routine, the motion correction algorithm needs to provide a precision that allows radiological diagnosis or is not compromising further processing strategies. Because of the robust threshold criterion, the concept of a separate motion detection module excludes any artificially introduced artefacts or noise from imperfections in continuous motion monitoring.

Slow Movements

In the given experimental setup, the subjects performed abrupt head movements. Slow movements, due to relaxing muscles for example, are yet another frequently observed motion-pattern. This would lead to a slowly

varying navigator signal with a risk of being undetected, since the detection algorithm is designed to compensate slow drifts stemming from system sources. To avoid that the linear regression cancels those slow movements, the slope of the linear regression used in the algorithm was limited to the maximal slope of 0.9%/min as observed during the phantom experiments. Thus, the linear regression is accepting specific motion possibly caused by system-induced signal drifts. The observed maximal system-induced slope is within the range of values obtained from modern clinical 3 T systems (corresponding studies have been conducted in the context of functional MRI, see e.g. Ref. 30).

Slow signal changes on top of system-induced drifts lead to a steeper slope which, at some point during the measurement, might exceed the threshold and detect the movement. This behavior is comparable to define a maximal motion which is accepted, where beyond that artefacts are likely to show up. Verification experiments, however, are difficult to conduct, because training subjects to perform such a movement with an acceptable precision is unfeasible. Motion phantom experiments could overcome this problem and could help to further explore and fine-tune the method.

Quantification of Motion Parameters

So far, we discussed only the detection of motion. Future work will aim at back-calculating and quantifying the absolute motion-parameters (translation and rotation) from the FID navigator signal changes. Bearing in mind that the navigator acquisition has no or negligible impact on the imaging procedure, this is a particularly attractive goal. Initial simulations and experiments (using an additional reference scan to provide spatial information about the location of the coil elements with respect to the head) indicate the feasibility of such an approach.

CONCLUSIONS

Extending previous work using FID navigators (20–23), we applied FID navigators from a high channel count head coil to detect subject head motion during structural MRI acquisitions. Proof-of-principle was given with an implementation in a MP-RAGE sequence, although the methodology is compatible with various other sequences without or with only negligible time penalty and interferences on the imaging procedures. The stability and characteristics of the technique were investigated in phantom experiments. Human experiments proved its reliability and robustness and exhibit sensitivity to motion that, if corrected, render images of high quality. The method is considered to be especially interesting for acquisitions schemes where no online registration can be performed, in particular long anatomical scans, scans with changing image properties like DTI, CE-enhanced perfusion, and spectroscopic acquisitions.

ACKNOWLEDGMENTS

The authors thank Bénédicte Mortamet for the quality rating of the images and Delphine Ribes for her help with the image postprocessing.

REFERENCES

1. Maas LC, Frederick BD, Renshaw PF. Decoupled automated rotational and translational registration for functional MRI time series data: the DART registration algorithm. Magn Reson Med 1997;37:131–139.
2. Thesen S, Heid O, Mueller E, Schad LR. Prospective acquisition correction for head motion with image-based tracking for real-time fMRI. Magn Reson Med 2000;44:457–465.
3. Tremblay M, Tam F, Graham SJ. Retrospective coregistration of functional magnetic resonance imaging data using external monitoring. Magn Reson Med 2005;53:141–149.
4. Zaitsev M, Dold C, Sakas G, Hennig J, Speck O. Magnetic resonance imaging of freely moving objects: prospective real-time motion correction using an external optical motion tracking system. Neuroimage 2006;31:1038–1050.
5. Glover GH, Pauly JM. Projection reconstruction techniques for reduction of motion effects in MRI. Magn Reson Med 1992;28:275–289.
6. Meyer CH, Hu BS, Nishimura DG, Macovski A. Fast spiral coronary artery imaging. Magn Reson Med 1992;28:202–213.
7. Pipe JG. Motion correction with PROPELLER MRI: application to head motion and free-breathing cardiac imaging. Magn Reson Med 1999;42:963–969.
8. Ehman RL, Felmlee JP. Adaptive technique for high-definition MR imaging of moving structures. Radiology 1989;173:255–263.
9. Fu ZW, Wang Y, Grimm RC, Rossman PJ, Felmlee JP, Riederer SJ, Ehman RL. Orbital navigator echoes for motion measurements in magnetic resonance imaging. Magn Reson Med 1995;34:746–753.
10. Welch EB, Manduca A, Grimm RC, Ward HA, Jack CR Jr. Spherical navigator echoes for full 3D rigid body motion measurement in MRI. Magn Reson Med 2002;47:32–41.
11. Kadah YM, Abaza AA, Fahmy AS, Youssef AB, Heberlein K, Hu XP. Floating navigator echo (FNAV) for in-plane 2D translational motion estimation. Magn Reson Med 2004;51:403–407.
12. Costa AF, Petrie DW, Yen YF, Drangova M. Using the axis of rotation of polar navigator echoes to rapidly measure 3D rigid-body motion. Magn Reson Med 2005;53:150–158.
13. Petrie DW, Costa AF, Takahashi A, Yen YF, Drangova M. Optimizing spherical navigator echoes for three-dimensional rigid-body motion detection. Magn Reson Med 2005;53:1080–1087.
14. White N, Roddey C, Shankaranarayanan A, Han E, Rettmann D, Santos J, Kuperman J, Dale A. PROMO: real-time prospective motion correction in MRI using image-based tracking. Magn Reson Med 2010;63:91–105.
15. van der Kouwe AJ, Benner T, Dale AM. Real-time rigid body motion correction and shimming using cloverleaf navigators. Magn Reson Med 2006;56:1019–1032.
16. Ward HA, Riederer SJ, Jack CR Jr. Real-time autoshimming for echo planar timecourse imaging. Magn Reson Med 2002;48:771–780.
17. Thiel T, Czisch M, Elbel GK, Hennig J. Phase coherent averaging in magnetic resonance spectroscopy using interleaved navigator scans: compensation of motion artifacts and magnetic field instabilities. Magn Reson Med 2002;47:1077–1082.
18. Haase A, Frahm J, Matthaei D, Hanicke W, Merboldt KD. Flash imaging rapid NMR imaging using low flip-angle pulses. J Magn Reson 1986;67:258–266.
19. Hennig J, Nauerth A, Friedburg H. RARE imaging: a fast imaging method for clinical MR. Magn Reson Med 1986;3:823–833.
20. Hu X, Kim SG. Reduction of signal fluctuation in functional MRI using navigator echoes. Magn Reson Med 1994;31:495–503.
21. Pfeuffer J, Van de Moortele PF, Ugurbil K, Hu X, Glover GH. Correction of physiologically induced global off-resonance effects in dynamic echo-planar and spiral functional imaging. Magn Reson Med 2002;47:344–353.
22. Splitthoff DN, Zaitsev M. SENSE shimming (SSH): a fast approach for determining B(0) field inhomogeneities using sensitivity coding. Magn Reson Med 2009;62:1319–1325.
23. Brau AC, Brittain JH. Generalized self-navigated motion detection technique: preliminary investigation in abdominal imaging. Magn Reson Med 2006;55:263–270.
24. Wiggins GC, Triantafyllou C, Potthast A, Reykowski A, Nittka M, Wald LL. 32-channel 3 Tesla receive-only phased-array head coil with soccer-ball element geometry. Magn Reson Med 2006;56:216–223.

25. Jack CR Jr, Bernstein MA, Fox NC, Thompson P, Alexander G, Harvey D, Borowski B, Britson PJ, J LW, Ward C, Dale AM, Felmlee JP, Gunter JL, Hill DL, Killiany R, Schuff N, Fox-Bosetti S, Lin C, Studholme C, DeCarli CS, Krueger G, Ward HA, Metzger GJ, Scott KT, Mallozzi R, Blezek D, Levy J, Debbins JP, Fleisher AS, Albert M, Green R, Bartzokis G, Glover G, Mugler J, Weiner MW. The Alzheimer's disease neuroimaging initiative (ADNI): MRI methods. J Magn Reson Imaging 2008;27:685–691.
26. Mortamet B, Bernstein MA, Jack CR Jr, Gunter JL, Ward C, Britson PJ, Meuli R, Thiran JP, Krueger G. Automatic quality assessment in structural brain magnetic resonance imaging. Magn Reson Med 2009; 62:365–372.
27. Van de Moortele PF, Pfeuffer J, Glover GH, Ugurbil K, Hu X. Respiration-induced B0 fluctuations and their spatial distribution in the human brain at 7 Tesla. Magn Reson Med 2002;47:888–895.
28. Tisdall MD, Hess A, van der Kouwe AJ. MPRAGE using EPI navigators for prospective motion correction. In Proceedings of the 18th Annual Meeting of ISMRM, Honolulu, Hawai'i, USA, 2009. p 4656.
29. Maclaren J, Speck O, Stucht D, Schulze P, Hennig J, Zaitsev M. Navigator accuracy requirements for prospective motion correction. Magn Reson Med 2010;63:162–170.
30. Friedman L, Glover GH. Report on a multicenter fMRI quality assurance protocol. J Magn Reson Imaging 2006;23:827–839.